ACS APPLIED MATERIALS & INTERFACES

Research Article

www.acsami.org

Cell Microenvironment-Controlled Antitumor Drug Releasing-Nanomicelles for GLUT1-Targeting Hepatocellular Carcinoma Therapy

Yubo Guo,[†] Yujie Zhang,[†] Jianfeng Li,[†] Yu Zhang,[†] Yifei Lu,[†] Xutao Jiang,[†] Xi He,[†] Haojun Ma,[†] Sai An,[†] and Chen Jiang*[,†,‡]

[†]Key Laboratory of Smart Drug Delivery, Ministry of Education, Department of Pharmaceutics, School of Pharmacy, Fudan University, 826 Zhangheng Road, Shanghai 201203, China

[‡]State Key Laboratory of Medical Neurobiology, Fudan University, 138 Yixueyuan Road, Shanghai 200032, China

Supporting Information

ABSTRACT: In clinical therapy, the poor prognosis of hepatocellular carcinoma (HCC) is mainly attributed to the failure of chemotherapeutical agents to accumulate in tumor as well as their serious systemic toxicity. In this work, we developed actively tumor-targeting trilayer micelles with microenvironment-sensitive cross-links as a novel nanocarrier for HCC therapy. These micelles comprised biodegradable PEG-*p*Lys-*p*Phe polymers, in which *p*Lys could react with a disulfide-containing agent to form redox-responsive cross-links. In vitro drug release and pharmacokinetics studies showed that these cross-links were stable in physiological condition whereas cleaved once internalized into cells due to the high level of glutathione, resulting in facilitated intracellular doxorubicin release. In addition, dehydroascorbic acid (DHAA) was decorated on the surface of micelles for specific recognition of tumor cells via GLUT1, a member of glucose transporter family overexpressed on hepatocarcinoma cells. Moreover, DHAA exhibited a "one-way" continuous accumulation within tumor cells. Cellular uptake and in vivo imaging studies proved that these micelles had remarkable targeting property toward hepatocarcinoma cells and tumor. Enhanced anti-HCC efficacy of the micelles was also confirmed both in vitro and in vivo. Therefore, this micellar system may be a potential platform of chemotherapeutics delivery for HCC therapy.

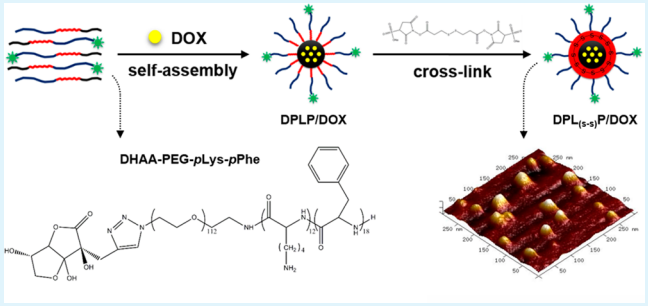

KEYWORDS: *polymer micelle, dehydroascorbic acid, GLUT1, cross-link, redox-responsive, hepatocellular carcinoma*

1. INTRODUCTION

Hepatocellular carcinoma (HCC) is the fifth most frequent neoplasm and the second leading cancer-associated mortality worldwide.[1−3] Despite the application of surgical management and other therapeutic modalities, the overall prognosis of HCC patients is dismal and the incidence of HCC continues to rise.[4−6] Doxorubicin (DOX), an anthracycline antibiotic, is one of the most widely used and effective chemotherapeutic agent for the treatment of HCC.[7−9] However, there are numerous limitations that restrict the clinical use of DOX, such as poor solubility, quick clearance and severe systemic toxicity to normal tissues.[10,11]

Nowadays, polymer micelles have attracted an increasing interest in cancer therapy for the sake of improving solubility and bioavailability of hydrophobic antitumor drugs and prolonging blood circulation by resisting rapid renal clearance.[12−15] Moreover, micelles with a diameter under 100 nm can passively accumulate in tumor tissue via enhanced permeability and retention (EPR) effect, a unique anatomical-pathophysiological property of tumor blood vessels.[16,17] Unfortunately, most micelles are still facing tremendous challenges, including lack of structural stability in blood circulation, nonspecific cellular internalization, and inefficient intracellular drug release.[18,19]

Unstable micelles may undergo a premature leak of encapsulated drugs, leading to loss of cytotoxic agents in blood circulation and undesired tissues. Therefore, the stability of micelles may be the prerequisite for accurate delivery of entrapped drugs to target sites. To date, covalent cross-linking of polymer micelles is a research hotspot of great significance for it can prevent disassembly related drug loss.[20,21] As known, glutathione (GSH) is a crucial intracellular reductant and can cleave disulfide efficiently. It is noteworthy that the substantial intracellular concentration of GSH (~10 mM) is approximately 5000-fold higher than the level in extracellular environments (~2 μM).[22] More importantly, there also exists an increased concentration of GSH (>4-fold) in tumor region compared with normal tissues.[23] This dramatic difference in GSH level

Received: December 29, 2014
Accepted: February 16, 2015
Published: February 16, 2015

ACS Publications © 2015 American Chemical Society

DOI: 10.1021/am5091462
ACS Appl. Mater. Interfaces 2015, 7, 5444−5453

can be utilized as a trigger for redox-sensitive drug release inside the target cells. Thus, the introduction of GSH-triggered disulfide cross-links into polymer micelles may stabilize the structure of micelles in blood circulation and initiate drug release efficiently once internalized into target cells.

To facilitate the cellular uptake of micelles, modifying various target ligands on the surface of micelles to improve internalization via receptor-mediated transport is a common approach.[24,25] In recent years, several transporters have been found to be overexpressed on the membrane of tumor cells in order to satisfy excess nutritional requirements of tumors.[26,27] Compared with receptor-mediated transport, transporter-mediated pathway is more rapid and efficient in transportation of small molecules. Facilitative glucose transporter isoform 1 (GLUT1) is a representative member of the GLUT family which is mainly responsible for "two-way" transportation of D-glucose across the membrane to keep an appropriate concentration in cells.[28] Known as Warburg effect,[29] tumor cells exhibit a huge consumption of glucose for proliferation in hypoxic environment.[30,31] It has been proven that GLUT1 is overexpressed on most hepatocarcinoma cells.[32,33] Moreover, GLUT1 expressed on tumor cells exhibits higher transport rate (V_{max}) compared with that on normal cells.[34] Dehydroascorbic acid (DHAA), structurally similar to D-glucose, is also a substrate of GLUT1.[35,36] Different from D-glucose, DHAA is rapidly reduced to ascorbic acid (AA) once internalized into cells. This structure transform helps DHAA escape the efflux and maintain a concentration gradient to drive DHAA to be taken into cells constantly because AA cannot be regognized by GLUT1.[37] Therefore, DHAA shows a "one-way" continuous accumulation in target cells. This incomparable superiority makes DHAA a potential functional moiety to enhance the hepatocarcinoma cell accumulation of micelles.

In this work, we, for the first time, developed DHAA-modified disulfide cross-linked micelles combining high plasma stability, hepatocarcinoma cell-targeting ability and GSH-triggered drug release behavior to achieve effective HCC therapy as well as low toxicity to normal tissues (Scheme 1). PEG-*p*Lys-*p*Phe was synthesized as an amphiphilic triblock polymer, which is biodegradable, nontoxic and easy to modify, to load chemotherapeutic agent DOX. The cross-link barrier was constituted through a reaction of amino groups on side chains of *p*Lys with a disulfide containing agent. DHAA was covalently anchored on the surface of micelles as the target ligand. The stability, tumor-targeting capacity and anti-HCC efficacy of these micelles were investigated in vitro and in vivo.

Scheme 1. Illustration of Stepwise Synthesis, GLUT1-Mediated Endocytosis, and GSH-Triggered Intracellular Drug Release of DPL$_{(s-s)}$P/DOX Micelles

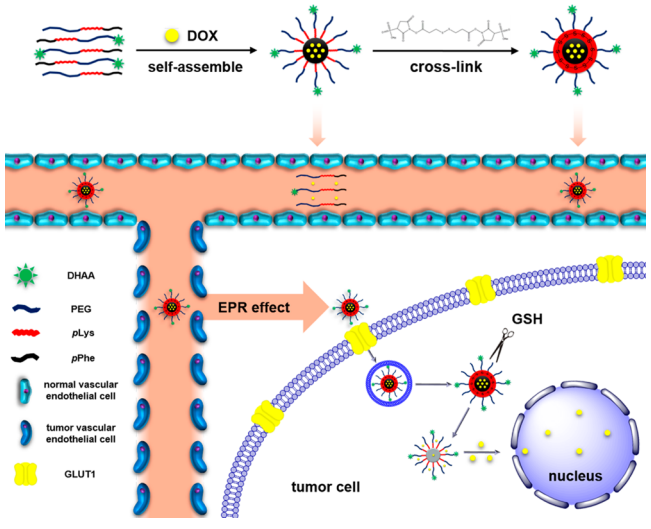

2. MATERIALS AND METHODS

2.1. Materials. N^6-Carbobenzyloxy-L-lysine (Lys(Z)), L-phenylalanine (Phe), and triphosgene were purchased from TCI (Tokyo, Japan). *N*,*N*-Dimethylformamide (DMF), tetrahydrofuran (THF) and *n*-hexane of extra dry over molecular sieve were purchased from Acros Organics (Geel, Belgium). Trifluoroacetic acid (TFA), 33% hydrogen bromide in acetic acid (HBr/HOAc), D-glucose, phenylarine oxide, filipin complex, colchicine and 3-(4,5-dimethyl-2-thiazolyl)-2,5-diphenyl-2H tetrazolium bromide (MTT) were purchased from Sigma-Aldrich (St. Louis, MO, USA). α-Methoxy-ω-amino-poly(ethylene glycol) (*m*PEG-NH_2, MW 5000) was purchased from Seebio Biotech (Shanghai, China). α-Azide-ω-amino-poly(ethylene glycol) (N_3-PEG-NH_2, MW 5000) was purchased from Jenkem Technology (Beijing, China). Doxorubicin hydrochloride (DOX·HCl) was purchased from Meilun Biotech (Dalian, China). 3,3′-Dithiobis(sulfosuccinimidylpropionate) (DTSSP) was purchased from Thermo Pierce (Rockford, IL, USA). 4,6-Diamidino-2-phenylindole (DAPI) was purchased from Molecular Probes (Eugene, OR, USA). One Step TUNEL Apoptosis Assay Kit was purchased from KeyGEN BioTECH (Nanjing, China). RPMI Medium 1640 and fetal bovine serum (FBS) was purchased from Gibco (Tulsa, OK, USA). Near infrared fluorescent probe IR783 was kindly provided by Prof. Cong Li (Molecular Imaging Institute, School of Pharmacy, Fudan University). Other reagents, if not specified, were purchased from Sinopharm Chemical Reagent (Shanghai, China).

Bel-7402 human hepatocarcinoma cells were purchased from Cell Bank, Chinese Academy of Sciences (Shanghai, China). Bel-7402 cells were maintained in RPMI Medium 1640 supplemented with 10% heat-inactivated FBS, 100 U/mL penicillin and 100 μg/mL streptomycin and cultured at 37 °C under a humidified atmosphere containing 5% CO_2.

Male Balb/c nude mice of ~20 g body weight and male SD rats of ~200 g body weight were purchased from Department of Experimental Animals, Fudan University and maintained under standard laboratory conditions. For construction of subcutaneous xenograft model, 3×10^6 Bel-7402 cells in 100 μL PBS (pH 7.2) were inoculated subcutaneously in the proximal right femur region of a nude mouse. All animal experiments were carried out in accordance with guidelines evaluated and approved by the ethics committee of Fudan University.

2.2. Synthesis of Monomers. Synthesis of N^6-carbobenzyloxy-L-lysine *N*-carboxyanhydride (Lys(Z)-NCA) and L-phenylalanine *N*-carboxyanhydride (Phe-NCA) was carried out by Fuchs−Farthing method using triphosgene (Figure S1 in the Supporting Information).[38]

2.3. Synthesis of Polymers. *m*PEG-*p*Lys-*p*Phe triblock polymer, comprising EG units of 112 (MW 5000), Lys units of 12 and Phe units of 18, was synthesized via ring-opening polymerization (ROP) reaction (Figure S2 in the Supporting Information). N_3-PEG-*p*Lys-*p*Phe polymer was synthesized by the same procedure, with N_3−PEG-NH_2 (MW 5000) as the initiator. In brief, To a stirred solution of PEG (1 g, 0.2 mmol) in anhydrous DMF (10 mL) was added Lys(Z)-NCA (736 mg, 2.4 mmol) at 50 °C under nitrogen. After 48 h, Phe-NCA (1.15 g, 6 mmol) in anhydrous DMF (20 mL) was added to the reaction mixture, and the reaction was maintained for another 48 h. The polymer was isolated by repeated precipitation from DMF into diethyl ether and was vacuum-dried to yield off-white solid. Finally, the deprotection of PEG-*p*Lys(Z)-*p*Phe was performed by treating the polymer (1 g) with TFA (10 mL) and HBr/HOAc (0.5 mL) to remove Z groups. The product, PEG-*p*Lys-*p*Phe, was isolated by dialysis using a membrane (Spectrapor, molecular weight cutoff (MWCO): 1000) for 24 h, followed by freeze-drying. The preparation

DOI: 10.1021/am5091462
ACS Appl. Mater. Interfaces 2015, 7, 5444−5453

of near-infrared fluorescent probe IR783-labeled PEG-*p*Lys-*p*Phe was achieved by the reaction of amino groups on side chains of *p*Lys with active groups NHS contained in IR783. Briefly, PEG-*p*Lys-*p*Phe was dissolved in anhydrous DMF with IR783 (0.1 equiv) and DIEA (0.5 equiv). The reaction was maintained at room temperature for 2 h in darkness and the product was obtained by further dialysis and freeze-drying.

DHAA was coupled to the terminus of N_3−PEG-*p*Lys-*p*Phe via copper(I)-catalyzed azide−alkyne Click reaction (Figure S2 in the Supporting Information).[39] N_3-PEG-*p*Lys-*p*Phe and 2-propargyl DHAA (2 equiv) were dissolved in DMF under nitrogen. A freshly prepared solution of CuI (0.5 equiv), sodium ascorbate (1 equiv), and DIEA (1 equiv) was added to the mixture and the reaction was carried out at 30 °C for 12 h. The product, DHAA-PEG-*p*Lys-*p*Phe, was purified by dialysis using a membrane (MWCO: 1000) against 10 mM EDTA-2Na (pH 7.0) for 24 h, deionized water for 24 h, followed by freeze-drying.

2.4. Preparation of Micelles. *m*PEG-*p*Lys-*p*Phe (10 mg) and DOX (1 mg) were dissolved in DMF (1 mL). The solution was dialyzed against deionized water for 24 h using a membrane (MWCO: 1000). Then DOX-loaded non-cross-linked micelles PLP/DOX were collected. DTSSP as a disulfide-containing cross-linking agent was then added to the solution at a feed molar ratio of [DTSSP]: [Lys] = 1:1. The reaction was maintained for 3 h at pH 8.0, and the solution was dialyzed against deionized water for 12 h to remove residual DTSSP, then DOX-loaded cross-linked micelles $PL_{(s\text{-}s)}P$/DOX were collected. For DHAA-modified micelles preparation, *m*PEG-*p*Lys-*p*Phe (8 mg), DHAA-PEG-*p*Lys-*p*Phe (2 mg) and DOX (1 mg) were dissolved in DMF (1 mL). The later procedure was the same as mentioned above, and then DPLP/DOX and $DPL_{(s\text{-}s)}P$/DOX micelles were collected.

Blank micelles and IR783-labeled micelles (containing 10 wt % of IR783-labeled *m*PEG-*p*Lys-*p*Phe) were prepared according to the procedure mentioned above without adding DOX into the initial mixture in DMF.

All of the prepared micelles were stored in 4 °C until use.

2.5. Characterizations. Synthetic monomers and copolymers were characterized by ^{1}H NMR spectra measured by NMR spectrometer (Bruker, Billerica, MA, USA), using tetramethylsilane (TMS) as internal reference and d_6-DMSO as solvent. Size/PDI and zeta-potential of prepared micelles were measured by dynamic light scattering (DLS) (Zetasizer Nano-ZS, Malvern, U.K.). The morphological examination of micelles was performed using atom force microscopy (AFM) (Bruker, Billerica, MA, USA). The critical micelle concentration (CMC) was obtained by luminescence spectrometer (PerkinElmer, Waltham, MA, USA) with pyrene as a fluorescent probe at 25 °C. DOX loading and encapsulation efficiency were obtained by microplate spectrophotometer (BioTek, Winooski, VT, USA).

2.6. In Vitro DOX Release Study. In vitro DOX release from DPLP/DOX and $DPL_{(s\text{-}s)}P$/DOX micelles was performed using dialysis method (n = 3). In brief, a 0.4 mL solution of micelles (0.5 mg DOX/mL) was placed in a dialysis bag (MWCO: 1000). The bag was clamped and suspended in a centrifuge tube containing 40 mL PBS (pH 7.4), which was shaken at 100 rpm at 37 °C, immediately. An aliquot of solution (0.5 mL) was withdrawn from the tube and 0.5 mL fresh PBS (pH 7.4) was replenished at various time points. The concentration of DOX was measured by microplate spectrophotometer at Ex/Em 480 nm/525 nm.

GSH-triggered in vitro DOX release from $DPL_{(s\text{-}s)}P$/DOX micelles was performed according to the same procedure mentioned above, using different concentrations (2 μM and 10 mM) of GSH contained PBS (pH 7.4) as dialysis medium.

2.7. Cellular Uptake and Internalization Mechanism Studies. Bel-7402 cells were seeded in 6-well plates (Corning-Coaster, Tokyo, Japan) at a density of 1×10^5 cells/well and incubated at 37 °C for 24 h. When 80% - 90% confluence was achieved, cells were washed and preincubated with D-glucose-free Hank's at 37 °C for 15 min. Then cells were incubated with free DOX, $PL_{(s\text{-}s)}P$/DOX micelles and $DPL_{(s\text{-}s)}P$/DOX micelles with different DHAA-PEG-*p*Lys-*p*Phe ratios (10, 20, and 40 wt %) at a concentration of 10 μg DOX/mL in D-glucose-free medium. To investigate the mechanism of internalization, we preincubated cells with D-glucose-free Hank's containing different inhibitors, including different concentrations of D-glucose (2 mM and 10 mM) as GLUT1 transporter inhibitors and 1 μg/mL colchicine, 0.4 μg/mL phenylarine oxide (PhAsO) and 0.5 μg/mL filipin complex as endocytic inhibitors, at 37 °C for 15 min. Then $DPL_{(s\text{-}s)}P$/DOX micelles at a concentration of 10 μg DOX/mL in D-glucose-free medium were introduced to cells. After 30 min, the medium was removed, cells were washed for three times and then visualized and photographed using fluorescence microscope (Leica, Wetzlar, Germany). For flow cytometry analysis, cells were digested, centrifuged, and washed twice with PBS (pH 7.2). The fluorescent intensity of DOX in cells was analyzed using flow cytometer (BD Biosciences, Bedford, MA, USA) at 488 nm excitation with 1×10^4 events collected for each analysis. Cells without any treatment were used as control.

2.8. In Vitro Cytotoxicity Study. In vitro cytotoxicity was assessed by MTT assay (n = 4). Briefly, Bel-7402 cells were seeded in 96-well plates at a density of 5×10^3 cells/well and incubated at 37 °C for 24 h. When 60−70% confluence was achieved, cells were washed and preincubated with D-glucose-free Hank's at 37 °C for 15 min. Then cells were incubated with free DOX, PLP/DOX, $PL_{(s\text{-}s)}P$/DOX, DPLP/DOX and $DPL_{(s\text{-}s)}P$/DOX micelles at various DOX concentrations in medium containing 2 mM D-glucose at 37 °C. After 48 h, the medium was removed and cells were washed for three times. Then 100 μL MTT solution (0.5 mg/mL) was added into each well and cells were incubated at 37 °C for 4 h. Next, the solution was removed and 100 μL DMSO was added into each well, followed by shaken for 10 min. The absorbance of formazan crystals was read at 570 nm using microplate spectrophotometer. Cells without treatment were served as control. In vitro cytotoxicity of polymers was assessed by the same procedure with different concentrations of polymers.

2.9. In Vivo Imaging Study. In vivo imaging study was performed in Bel-7402 tumor-bearing nude mice intravenously injected with IR783-labeled $PL_{(s\text{-}s)}P$ and $DPL_{(s\text{-}s)}P$ micelles at the same dose of 1 mg micelles per mouse. Then at 2 h, 4 h, 12 and 24 h after injection, mice were anesthetized, visualized and photographed under IVIS Spectrum in vivo image system (Caliper, Newton, MA, USA) at Ex/Em 768 nm/789 nm.

2.10. Pharmacokinetics and Biodistribution Studies. Pharmacokinetics study was performed in SD rats intravenously injected with free DOX, PLP/DOX, $PL_{(s\text{-}s)}P$/DOX, DPLP/DOX, and $DPL_{(s\text{-}s)}P$/DOX micelles at a dose of 5 mg DOX/kg (n = 5). Blood samples of each group were collected at various time points. Biodistribution study was performed in Bel-7402 tumor-bearing nude mice intravenously injected with free DOX, PLP/DOX, $PL_{(s\text{-}s)}P$/DOX, DPLP/DOX, and $DPL_{(s\text{-}s)}P$/DOX micelles at a dose of 5 mg DOX/kg (n = 4). After 24 h, mice were sacrificed and main organs and tissues (heart, liver, spleen, lung, kidney, brain and tumor) were excised and collected. These organs and tissues were washed, weighted and homogenized.

DOX concentration in blood or tissues was determined by HPLC.[40] In brief, blood samples or tissue homogenate were centrifuged twice (12 000 rpm, 5 min) and the supernate were collected. Then 200 μL methanol was added to 100 μL of the supernate to precipitate proteins, and the mixture was centrifuged twice (12 000 rpm, 5 min) to collect the supernate. Finally, 20 μL of each supernate was injected into HPLC (Agilent ODS C18 column (4.6 × 250 mm, 5 μm particle size), 10 mM KH_2PO_4: acetonitrile: acetic acid = 70:30:0.3 (v/v/v), 1.0 mL/min, 25 °C, Ex/Em = 480 nm/560 nm) for DOX quantification.

2.11. In Vivo Antitumor Efficacy Study. In vivo antitumor efficacy study was performed in Bel-7402 tumor-bearing nude mice intravenously injected three times (on days 0, 7, and 14) with free DOX, PLP/DOX, $PL_{(s\text{-}s)}P$/DOX, DPLP/DOX and $DPL_{(s\text{-}s)}P$/DOX micelles at a dose of 5 mg DOX/kg (n = 6). Mice treated with saline were served as control. The shortest diameter (s) and the longest diameter (l) of each tumor were measured by a digital caliper every other day and the tumor volume (V) was calculated according to the following formula: $V = s^2 l\pi/6$.[41] The body weight of mice was also measured every other day to evaluate the toxicity indirectly. On day

DOI: 10.1021/am5091462
ACS Appl. Mater. Interfaces 2015, 7, 5444−5453

18, all mice were euthanized and tumors were excised and photographed.

2.12. In Vivo Apoptosis Study. Tumors excised from mice on day 18 were fixed with 4% polyoxymethylene for 48 h, placed in 15% sucrose solution for 24 h until subsidence, then in 30% sucrose solution for 48 h until subsidence. Afterward, tumors were sectioned into sliced at a thickness of 10 μm at −20 °C. Slices were stained with TUNEL and DAPI, and then visualized and photographed using fluorescence microscope.

2.13. Statistical Analysis. Analysis was performed using GraphPad Prism software. Pharmacokinetic parameters were calculated by DAS software. Statistical comparisons were assessed by one-way ANOVA. Data are represented as mean ± SD.

3. RESULTS AND DISSCUSSION

3.1. Synthesis and Characterization of Polymers. PEG-ploy(amino acid) triblock polymers, *m*PEG-*p*Lys-*p*Phe and N_3-PEG-*p*Lys-*p*Phe, were synthesized via a one-pot two-step ring-opening polymerization (ROP) reaction in the presence of CH_3O-PEG-NH_2 and N_3-PEG-NH_2 as initiators and previously activated amino acids, Lys(Z)-NCA and Phe-NCA (Figure S1 in the Supporting Information), as monomers (Figure S2 in the Supporting Information). These polymers comprise three segments playing different roles in forming micelles: (1) polymeric Phe (*p*Phe), the hydrophobic core for encapsulating insoluble drugs; (2) polymeric Lys (*p*Lys), full of amino groups on side chains for cross-link; (3) PEG, the hydrophilic shell for prolonging circulation time in blood and conjugating target vectors.

The characteristic peaks of PEG at 3.54 ppm (methylene groups), Lys(Z) at 1.2−1.78 ppm (methylene groups on the side chain) and Phe at 4.5 ppm (methylene of benzyl group) were found in ^{1}H NMR spectra shown in Figure S3A, B in the Supporting Information. The molar composition ratio of PEG, Lys, and Phe in PEG-*p*Lys-*p*Phe was 1:12:18, and the conversion ratio of monomeric Lys(Z)-NCA and Phe-NCA to polymeric Lys(Z) and Phe was 100 and 60%, respectively. The steric hindrance of benzyl led to the lower conversion ratio of monomeric Phe compared with Lys(Z). The complete disappearance of the resonance peak at 5.01 ppm in Figure S3C in the Supporting Information indicated that Z groups were removed from Lys(Z) successfully. The molecular weight of polymers calculated by ^{1}H NMR spectra was 9187.28 g/mol. The critical micelle concentration (CMC) of polymers was 49.41 μg/mL.

Conjugation of DHAA to the end of N_3-PEG-*p*Lys-*p*Phe was performed via Click reaction, a widely used bioconjugation approach which is fast, highly efficient and completed under mild conditions.[42,43] 2-Propargyl DHAA could react with the azide moiety of N_3-PEG-*p*Lys-*p*Phe in the presence of Cu(I) as catalyst to form a triazole ring, which is quite stable in physiological conditions (Figure S2 in the Supporting Information). As shown in Figure S3D in the Supporting Information, the appearance of resonance peaks at 8.03 ppm indicated the formation of the triazole ring, which proved the successful conjugation of DHAA to N_3-PEG-*p*Lys-*p*Phe.

3.2. Preparation and Characterization of Micelles. DOX-loaded non-cross-linked micelles were prepared via dialysis method using DOX/polymers mixture. For DHAA-modified micelles, the quantitative addition of DHAA-PEG-*p*Lys-*p*Phe could control the modification density of DHAA on the surface of micelles.[44] Disulfide cross-linked micelles were prepared by adding DTSSP to a solution of non-cross-linked micelles. DTSSP is a water-soluble disulfide-containing cross-link agent with active *N*-hydroxysuccinimide (NHS) esters that can react with primary amines of *p*Lys to form intramicellar cross-linkes. Herein, four kinds of micelles were prepared: DOX-loaded non-cross-linked or cross-linked micelles (PLP/DOX or $PL_{(s\text{-}s)}P$/DOX), and DOX-loaded DHAA-modified non-cross-linked or cross-linked micelles (DPLP/DOX or $DPL_{(s\text{-}s)}P$/DOX).

The average hydrodynamic diameter and zeta potential of DPLP/DOX micelles was 60.34 nm and 23.7 mV, respectively (Figure 1A and Table 1). $DPL_{(s\text{-}s)}P$/DOX micelles had a

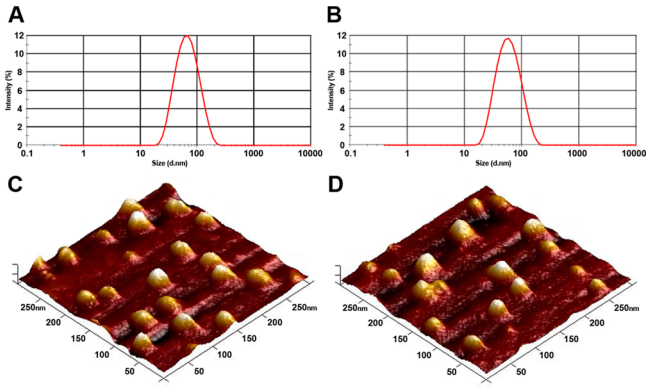

Figure 1. Size distribution of (A) DPLP/DOX and (B) $DPL_{(s\text{-}s)}P$/DOX micelles. AFM images of (C) DPLP/DOX and (D) $DPL_{(s\text{-}s)}P$/DOX micelles.

decreased diameter of 51.99 nm compared with DPLP/DOX micelles (Figure 1B and Table 1). This indicated that the structure of $DPL_{(s\text{-}s)}P$/DOX micelles became more condensed after cross-link, probably because the weakened electrostatic repulsion and reduced intermolecular distance between polymers owing to the cross-link process. The mean value of zeta potential of $DPL_{(s\text{-}s)}P$/DOX micelles also decreased to 5.09 mV (Table 1), which reflected the conversion of electropositive primary amines on *p*Lys to amide linkages during the cross-link reaction. AFM images showed that both of DPLP/DOX and $DPL_{(s\text{-}s)}P$/DOX micelles revealed spherical morphology with moderate dispersivity (Figure 1C and D). The low PDI (<0.2) also indicated a narrow size distribution of these micelles. There was no obvious aggregation caused by cross-link. Moreover, 2 weeks after prepared, the size of $DPL_{(s\text{-}s)}P$/DOX micelles still maintained approximate 60 nm with a narrow distribution, showing good stability under storage condition (Figure S4 in the Supporting Information). Other properties of prepared micelles were displayed in Table 1.

3.3. In Vitro DOX Release from Micelles. To investigate the prevention effect of cross-links on DOX leakage from micelles, we estimated DOX release from DPLP/DOX and $DPL_{(s\text{-}s)}P$/DOX micelles in PBS (pH 7.4). As shown in Figure 2A, DPLP/DOX micelles underwent an initial burst release, in which 30% of DOX was released within 1h. In contrast, no trend of fast release was observed on $DPL_{(s\text{-}s)}P$/DOX micelles and only 20% of DOX release was detected after 48h. This indicated that the cross-link could greatly stabilize micelles under physiological conditions. We supposed that the cross-link layer might act as a diffusion barrier and could efficiently minimize undesired DOX leakage from micelles. Next, we investigated if DOX release from $DPL_{(s\text{-}s)}P$/DOX micelles was facilitated in response to the intracellular GSH concentration

DOI: 10.1021/am5091462
ACS Appl. Mater. Interfaces 2015, 7, 5444−5453

Table 1. Summary of Micelle Properties[a]

micelles	PLP/DOX	$PL_{(s\text{-}s)}P$/DOX	DPLP/DOX	$DPL_{(s\text{-}s)}P$/DOX
size *d* (nm)	52.00 ± 0.06	43.66 ± 0.31	60.34 ± 1.00	51.99 ± 0.82
PDI	0.175 ± 0.002	0.194 ± 0.010	0.198 ± 0.008	0.186 ± 0.007
Zeta potential (mV)	21.9 ± 0.9	5.59 ± 0.25	23.7 ± 2.7	5.09 ± 0.11
DOX loading efficiency (%)	7.50 ± 0.18	6.96 ± 0.11	7.56 ± 0.27	7.13 ± 0.16
DOX encapsulation efficiency (%)	81.1 ± 2.0	74.8 ± 1.3	81.7 ± 3.2	76.8 ± 1.8

[a]Data are represented as mean ± SD (n = 3).

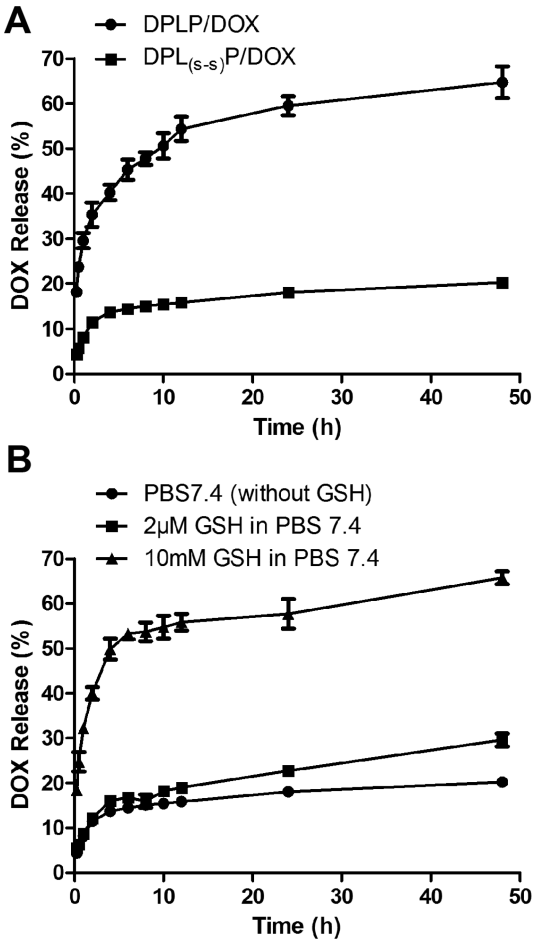

Figure 2. (A) In vitro DOX release from DPLP/DOX and $DPL_{(s\text{-}s)}P$/DOX micelles in PBS (pH 7.4) at 37 °C. (B) In vitro DOX release from $DPL_{(s\text{-}s)}P$/DOX micelles triggered by different concentrations of GSH in PBS (pH 7.4) at 37 °C. Data are represented as mean ± SD (n = 3).

level. Figure 2B exhibited DOX release profiles from $DPL_{(s\text{-}s)}P$/DOX micelles at different GSH concentrations. When exposed to a medium of extracellular GSH concentration (~2 μM), $DPL_{(s\text{-}s)}P$/DOX micelles remained relatively stable with only 30% of DOX release within 48 h. As the GSH concentration increased up to intracellular level (~10 mM), DOX release was markedly facilitated, where 40% of DOX was released within 2h and approximate 70% after 48h. This substantially accelerated DOX release from cross-linked micelles was likely attributed to the cleavage of disulfide linkages when exposed to cytoplasm level of GSH, which led to a loss of structural integrity and the following collapse of micelles.

3.4. Cellular Uptake and Internalization Mechanism of Micelles. We evaluated the cellular uptake characteristics and investigated the possible internalization mechanism of micelles in human hepatocarcinoma cell line Bel-7402 using fluorescence microscope to follow red signals from DOX, and quantitatively analyzed by flow cytometer (Figure 3).

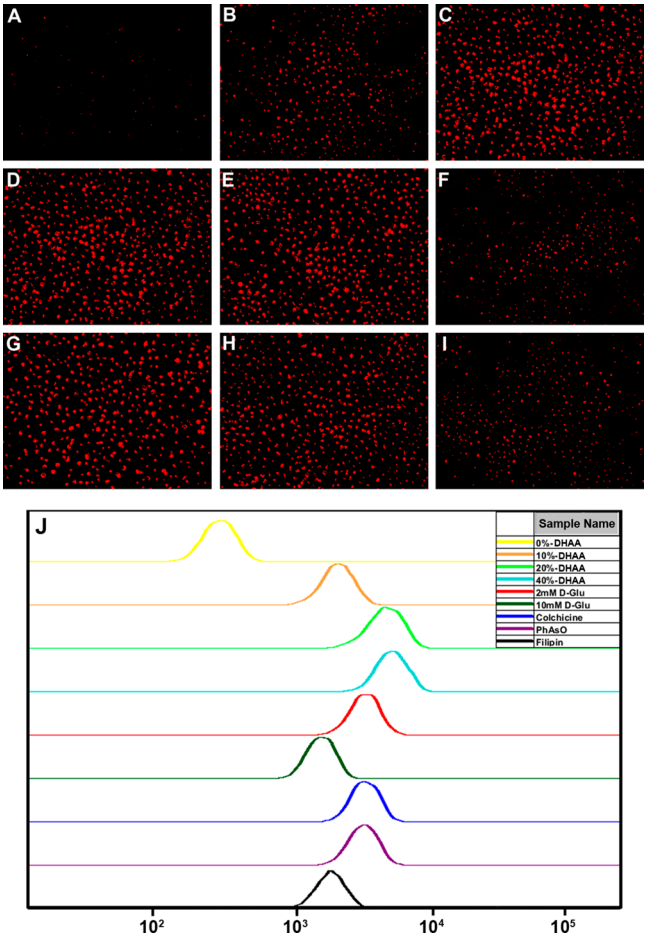

Figure 3. Cellular uptake of (A) $PL_{(s\text{-}s)}P$/DOX micelles and $DPL_{(s\text{-}s)}P$/DOX micelles with different DHAA-PEG-*p*Lys-*p*Phe ratios (B) 10, (C) 20, and (D) 40 wt % in Bel-7402 tumor cells 30 min after incubation. (E–I) Possible involved pathway of $DPL_{(s\text{-}s)}P$/DOX micelles internalization into Bel-7402 tumor cells. The cells were blocked by different inhibitors (E) 2 mM D-glucose, (F) 10 mM D-glucose, (G) 1 μg/mL Colchicine, (H) 0.4 μg/mL PhAsO, and (I) 0.5 μg/mL Filipin. Red, DOX; original magnification = 100×. (J) Flow cytometry analysis of A–I.

Compared with $PL_{(s\text{-}s)}P$/DOX micelles, the cellular uptake of $DPL_{(s\text{-}s)}P$/DOX micelles was significantly enhanced with increasing DHAA-PEG-*p*Lys-*p*Phe ratio (from 10 wt % to 40 wt %), suggesting that DHAA could improve the cellular uptake of micelles by Bel-7402 cells (Figure 3A–D and J). More importantly, DHAA-modified micelles even showed higher internalization than free DOX which enters cells via passive

DOI: 10.1021/am5091462
ACS Appl. Mater. Interfaces 2015, 7, 5444–5453

diffusion (Figure S5 in the Supporting Information). This notable phenomenon could be attributed to the remarkable higher expression and accelerated transport rate of GLUT1 on tumor cells. Additionally, we found that there was no significant difference between cellular uptakes of $DPL_{(s-s)}P$/DOX micelles with DHAA-PEG-*p*Lys-*p*Phe ratio of 20 and 40 wt %, probably because the transport capacity of GLUT1 had reached saturation. In consideration of systemic long circulation, we chose micelles with DHAA-PEG-*p*Lys-*p*Phe ratio of 20 wt % as $DPL_{(s-s)}P$/DOX micelles in following studies.

To investigate the possible internalization mechanism of $DPL_{(s-s)}P$/DOX micelles, we inhibited the cellular uptake by various inhibitors, including D-glucose (blocking GLUT1), colchicine (blocking macropinocytosis), phenylarsine oxide (blocking clathrin-dependent pathway) and filipin complex (blocking caveolae-mediated pathway) (Figure 3E–J). Notably, low concentration of D-glucose (2 mM) exhibited minor effect on the internalization of $DPL_{(s-s)}P$/DOX micelles (Figure 3E, J). However, the inhibition effect was enhanced as the concentration of D-glucose increased up to a high level (10 mM) (Figure 3F, J). Among the three endocytic inhibitors, filipin complex exhibited the most significant inhibition effect, indicating that the main endocytosis pathway of $DPL_{(s-s)}P$/DOX micelles was caveolae-mediated endocytosis, which is different from the conventional receptor-mediated clathrin-dependent endosome route (Figure 3G–J).[45,46] Considering these results above, we suggested that DHAA was mainly responsible for actively recognizing and binding to hepatocarcinoma cells through GLUT1, and the intrinsic properties of micelles, such as size, shape and charge, played a critical role in their internalization.

3.5. In Vitro Cytotoxicity Detection. In vitro cytotoxicity of free DOX and different DOX-loaded micelles against Bel-7402 cells was estimated by MTT assay to determine IC_{50} values (Figure 4B and Table 2). Blank micelles showed no cytotoxicity against Bel-7402 cells with the concentration of polymers ranging from 10 μg/mL to 2 mg/mL (Figure 4A). Poly(amino acid) polymers comprise endogenic L-amino acids connected through peptide bonds which can be cleaved by the peptidase system of human body own. Their degradation products are also nontoxicity. Therefore, these synthetic polymers can be seen as a kind of biodegradable material with high safety. Figure 4B revealed that different DOX formulations inhibited cell viability in a dose-dependent manner. As shown in Table 2, PLP/DOX (IC_{50} = 1.099 μg/mL) and $PL_{(s-s)}P$/DOX (IC_{50} = 1.033 μg/mL) micelles exhibited relatively low cytotoxicity compared with free DOX (IC_{50} = 0.846 μg/mL). This was because free DOX and micelles had different pathways to enter cells. Free DOX could enter cells via passive diffusion more easily while micelles were mainly internalized through endocytosis. $DPL_{(s-s)}P$/DOX micelles possessed the lowest IC_{50} value of 0.422 μg/mL, only half of free DOX, showing the most pronounced cytostatic activity. Given that DOX causes cytotoxicity through inhibiting DNA replication, we attributed this high potency to dramatically promoted endocytosis of DHAA-modified micelles, burst intracellular DOX release triggered by high concentration of GSH and the following abundant DOX diffusion into nucleus within a short time, causing suddenly intensive toxicity.

3.6. In Vivo Tumor Accumulation of Micelles. To further verify the tumor-targeting capacity of micelles, we intravenously injected near-infrared fluorescent probe IR783-

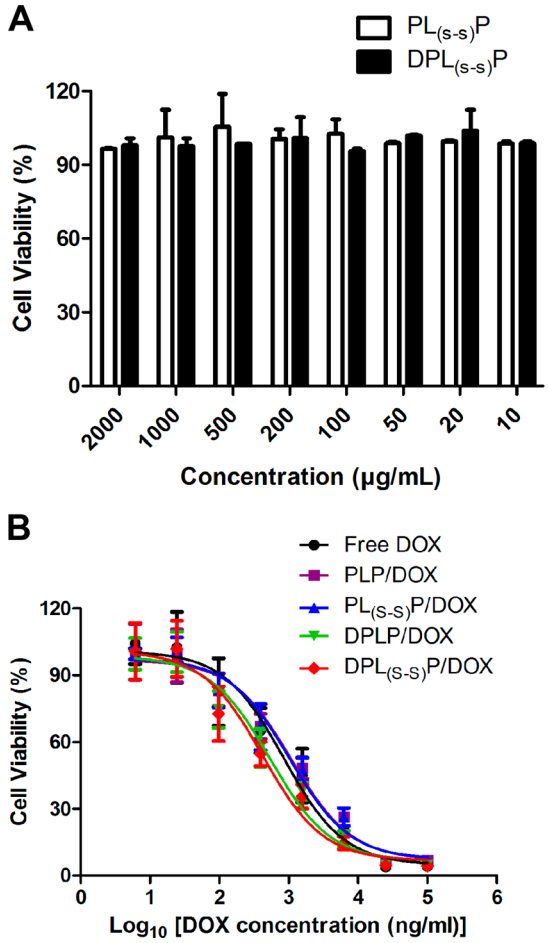

Figure 4. (A) Cell viability of Bel-7402 tumor cells after incubated with different concentrations of blank micelles for 48 h. (B) In vitro cytotoxicity of different DOX formulations at various concentrations against Bel-7402 tumor cells 48 h after incubation. Data are represented as mean ± SD (n = 4).

Table 2. IC_{50} Values of Different DOX Formulations against Bel-7402 Tumor Cells

formulations	IC_{50} (μg/mL)
free DOX	0.846
PLP/DOX	1.099
$PL_{(s-s)}P$/DOX	1.033
DPLP/DOX	0.537
$DPL_{(s-s)}P$/DOX	0.422

labeled $PL_{(s-s)}P$ and $DPL_{(s-s)}P$ micelles into Bel-7402 tumor-bearing mice and observed a real-time distribution of micelles under in vivo image system (Figure 5). Within 2 h after injection, most of the IR783-labeled $PL_{(s-s)}P$ and $DPL_{(s-s)}P$ micelles spread all over the body while a small fraction accumulated in liver (Figure 5A). Then, fluorescent signals were gradually enhanced in tumor region of the $DPL_{(s-s)}P$ micelles treated mouse, and became the strongest at 4 h (Figure 5B). Compared with $PL_{(s-s)}P$ micelles, $DPL_{(s-s)}P$ micelles exhibited much more tumor accumulation from 4 to 24 h after injection (Figure 5B - D). This indicated that DHAA maintained high tumor-targeting capacity in vivo and could promote micelles gradually accumulating in tumor cells. More importantly, the 3D image of the $DPL_{(s-s)}P$ micelles treated mouse at 24 h showed that a portion of micelles were localized

DOI: 10.1021/am5091462
ACS Appl. Mater. Interfaces 2015, 7, 5444–5453

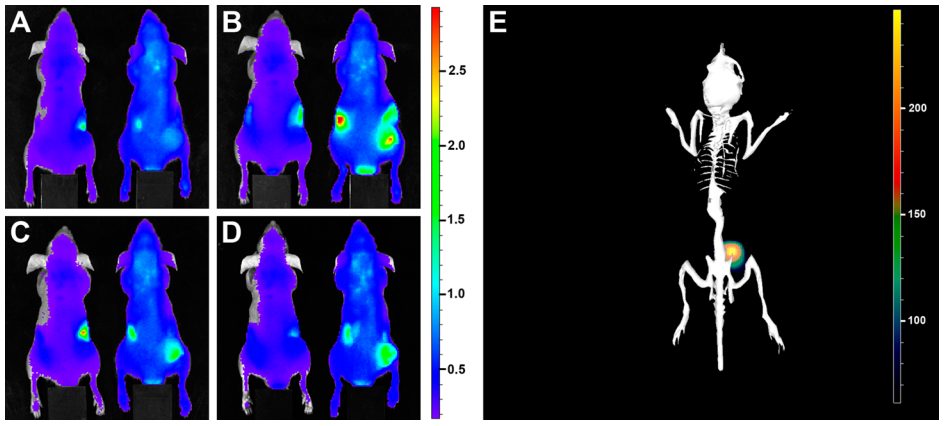

Figure 5. In vivo noninvasive NIR fluorescence imaging of Bel-7402 tumor-bearing nude mice at (A) 2, (B) 4, (C) 12, and (D) 24 h after i.v. injection with IR783-labeled $PL_{(s\text{-}s)}P$ (the left one in every image) and $DPL_{(s\text{-}s)}P$ (the right one in every image) micelles. (E) In vivo 3D fluorescence imaging of Bel-7402 tumor-bearing nude mouse at 24 h after i.v. injection with IR783-labeled $DPL_{(s\text{-}s)}P$ micelles.

in the central region of tumor (Figure 5E). As is well-known, it is quite difficult for chemotherapeutic drugs to deeply penetrate into the central region of tumor because of the high pressure and hypoxia.[47] Recently, it has been reported that the expression of GLUT1 was highly up-regulated in the intratumor region as tumor developed.[48] Combining the encouraging results above, DHAA could provide a promising way to increase the tumor penetration ability of micelles. Additionally, fluorescent signals could be distinctly observed in the whole body of mice up to 24 h, reflecting the improved stability of micelles attributed to the cross-link process.

3.7. Pharmacokinetics and Biodistribution Studies. To investigate whether the disulfide cross-link barrier could really shield the drug leakage from micelles during blood circulation, we studied the pharmacokinetic profiles of various DOX formulations. As shown in Figure 6, there was no significant

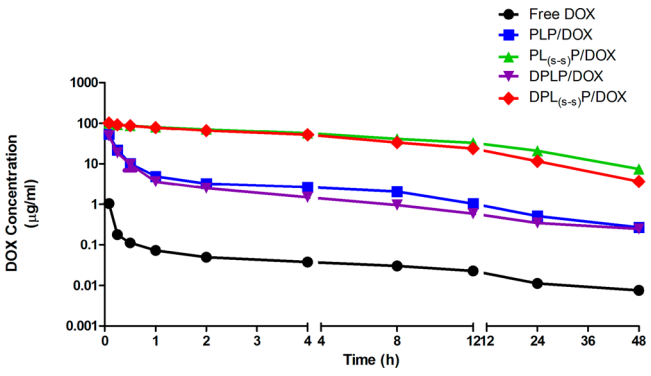

Figure 6. Pharmacokinetic profiles of DOX in SD rats after i.v. injection with different DOX formulations at a dose of 5 mg DOX/kg. Data are represented as mean ± SD (n = 5).

difference in pharmacokinetic profiles between DHAA modified and unmodified micelles. However, it showed that there were great changes in circulation behavior among free DOX, cross-linked and non-cross-linked micelles treated rats. As known, free DOX has a quite low binding rate with plasma proteins and shall distributes into extravascular tissues promptly once intravenously injected.[49] It was obvious that the clearance of DOX from blood became slower once loaded into micelles. Table 3 illustrated that cross-linked micelles (DHAA modified and unmodified) provided extremely higher $AUC_{(0\text{-}\infty)}$ (32-fold

Table 3. Pharmacokinetic Parameters of DOX in SD Rats after i.v. Injection with Different DOX Formulations at a Dose of 5 mg DOX/kg[a]

formulations	$t_{1/2\beta}$ (h)	$AUC_{(0\text{-}\infty)}$ (μg/(mL h))
Free DOX	2.810 ± 0.623	0.854 ± 0.103
PLP/DOX	5.910 ± 0.317	59.411 ± 6.673
$PL_{(s\text{-}s)}P$/DOX	16.437 ± 1.894	1469.336 ± 69.359
DPLP/DOX	4.822 ± 0.401	30.861 ± 1.240
$DPL_{(s\text{-}s)}P$/DOX	12.818 ± 0.738	965.373 ± 59.155

[a]Data are represented as mean ± SD (n = 5).

and 25-fold respectively) and much longer $t_{1/2\beta}$ (2.6-fold and 2.8-fold, respectively) than non-cross-linked micelles. This was probably because more DOX leaked out from destabilized non-cross-linked micelles upon blood dilution and then might be eliminated rapidly, while cross-linked micelles exhibited significantly increased resistance to blood dilution. All these findings demonstrated that cross-linked micelles could remain high integrity and stability during blood circulation and protect DOX being further metabolized and eliminated.

Next, we estimated the biodistribution profiles of various DOX formulations in principal organs and tissues of Bel-7402 tumor-bearing mice 24 h after injection. As shown in Figure 7, cross-linked micelles exhibited much higher accumulation in

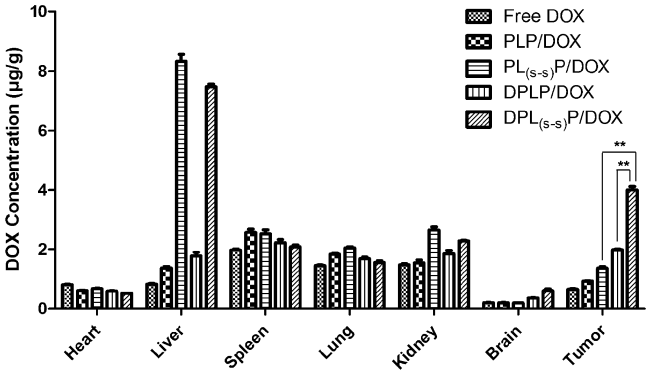

Figure 7. Distribution profiles of DOX in tissues of Bel-7402 tumor-bearing nude mice 24 h after i.v. injection with different DOX formulations at a dose of 5 mg DOX/kg. Data are represented as mean ± SD (n = 4), ** indicates $P < 0.01$.

DOI: 10.1021/am5091462
ACS Appl. Mater. Interfaces 2015, 7, 5444−5453

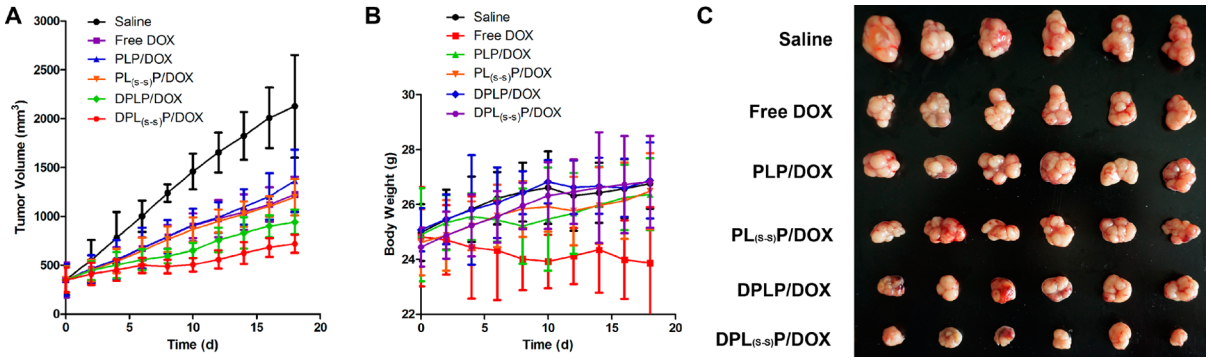

Figure 8. (A) Tumor volume changes and (B) body weight changes of Bel-7402 tumor-bearing nude mice after i.v. injection three times with different DOX formulations at a dose of 5 mg DOX/kg on days 0, 7, and 14. The saline treated group was served as control. Data are represented as mean ± SD (n = 6). (C) Excised tumors from Bel-7402 tumor-bearing nude mice at day 18 after the first injection.

liver compared with non-cross-linked micelles. It is undisputed that certain scale of intact micelles may be detained in liver through nonspecific uptake by RES phagocytic cells. Moreover, the remarkable liver accumulation was, to some extent, attributed to the properties of micelles composed of PEG-ploy(amino acid) polymers. It has been reported that the main metabolic pathway of this kind of micelles was through liver.[50] Notably, cross-linked micelles showed much higher accumulation in tumor ($P < 0.01$) and relative lower distribution in other organs after modified with DHAA. It was demonstrated that the distribution of micelles in vivo were altered after DHAA modification. Moreover, $DPL_{(s-s)}P/DOX$ micelles were almost twice as much as DPLP/DOX micelles in tumor region ($P < 0.01$), showing that reduced drug loss in blood would benefit for increased drug accumulation in tumor. Finally, among all of the harvested hearts, the mean level of detected DOX in $DPL_{(s-s)}P/DOX$ micelles treated mice was the lowest, which was particularly attractive because of the cardiotoxicity of DOX. Consequently, $DPL_{(s-s)}P/DOX$ micelles, as a DOX delivery system, could help reduce its side effect at the same time.

3.8. In Vivo Antitumor Efficacy Study. To assess the in vivo antitumor effects of micelles, Bel-7402 tumor-bearing mice were injected with various DOX formulations on days 0, 7, and 14. On day 18, all mice were sacrificed and tumors were excised. Figure 8A showed the tumor volume changes during the experiment and Figure 8C showed the size of excised tumors at the end of the experiment. Overall, tumor growth was inhibited in all DOX treated mice compared with the control. There was a limited inhibition of tumor growth in mice treated with free DOX, PLP/DOX and $PL_{(s-s)}P/DOX$ micelles attributed to lack of tumor targeting and/or rapid clearance from body. However, compared with unmodified micelles treated mice, DHAA-modified micelles treated mice exhibited markedly smaller tumor size. $DPL_{(s-s)}P/DOX$ micelles treated mice possessed a highest tumor inhibition ratio of 66% compared with the control at the end of the experiment. In addition, all of the micelles treated mice displayed an increase in body weight, whereas the free DOX group showed an obvious decrease due to the serious side effect of DOX (Figure 8B). All of these findings further confirmed that the cross-link barrier stabilized the micelles and decrease the leakage of DOX in blood, whereas DHAA modification altered the biodistribution of micelles and increased DOX accumulation in tumor region, resulting in remarkable antitumor efficacy and body safety.

3.9. Histological Analysis. TUNEL immunohistological assay was carried out to further evaluate the in vivo antitumor effects, which visualized apoptotic cells in tumors excised on day 18. Figure 9 showed images of DAPI staining (blue, nuclei),

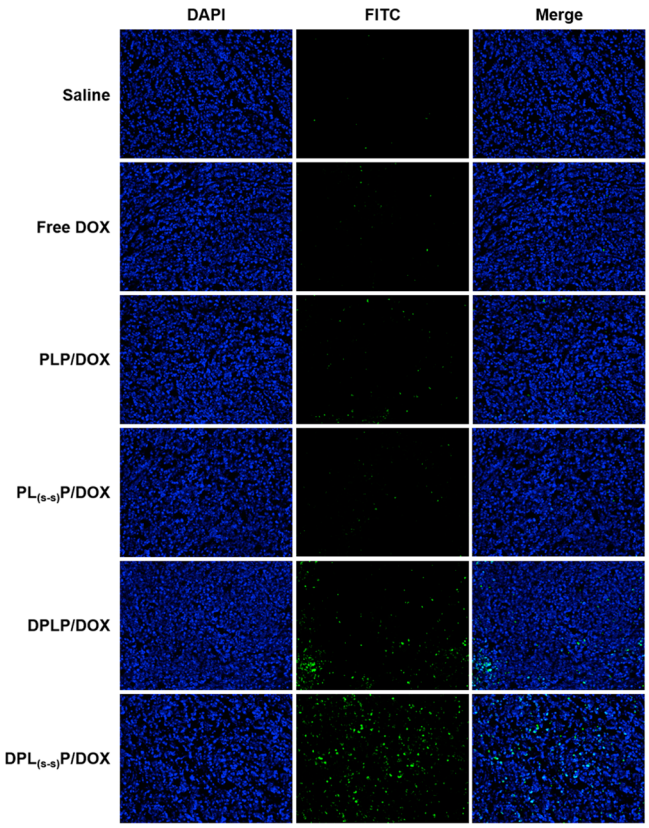

Figure 9. Representative histological images of Bel-7402 tumor xenografts excised from those nude mice used in the experiment of in vivo antitumor efficacy of micelles. Blue, DAPI-stained cell nuclei; green, apoptosis cells; original magnification = 100×.

TUNEL staining (green, apoptotic cells) and the merge of the two images. Apoptotic cells were barely detected in tumors of free DOX and unmodified micelles treated mice, but clearly present in tumors of DHAA-modified micelles treated mice. Notably, most apoptotic cells were found in tumors of $DPL_{(s-s)}P/DOX$ micelles treated mice. This was consistent with the results of in vivo antitumor efficacy. In addition, it is well-known that the proposed mechanism of antimalignancy of

DOI: 10.1021/am5091462
ACS Appl. Mater. Interfaces 2015, 7, 5444−5453

DOX is to insert into DNA leading DNA damage and eventually induce apoptosis.[51] The extensive tumor cell apoptosis caused by $DPL_{(s-s)}P$/DOX micelles could be partially attributed to the facilitated intracellular DOX release into cytoplasm and the subsequent entrance to the nucleus.

4. CONCLUSIONS

In summary, we developed DHAA-modified disulfide cross-linked DOX-loaded $DPL_{(s-s)}P$/DOX micelles for efficient therapy of HCC in our study. This smart drug delivery system can meet major requirements of micelles with high antitumor efficacy and low systemic toxicity: (i) high stability and minimized drug leakage in blood due to disulfide cross-links, (ii) prolonged in vivo circulation owing to the PEG outer shell, (iii) enhanced tumor accumulation by EPR effect, (iv) improved hepatocarcinoma cell-targeting and internalization due to DHAA modification, (v) facilitated intracellular drug release as a result of the cleavage of disulfides by GSH, (vi) favorable biocompatibility due to nontoxic PEG and amino acids. Therefore, these micelles have greatly potential applications in HCC therapy.

■ ASSOCIATED CONTENT

Supporting Information

Synthetic routes and ^{1}H NMR spectra of Lys(Z)-NCA, Phe-NCA, *m*PEG-*p*Lys(Z), *m*PEG-*p*Lys(Z)-*p*Phe, *m*PEG-*p*Lys-*p*Phe, and DHAA-PEG-*p*Lys-*p*Phe; size distribution of $DPL_{(s-s)}P$/DOX micelles under storage condition; cellular uptake of free DOX in Bel-7402 tumor cells. This material is available free of charge via the Internet at http://pubs.acs.org.

■ AUTHOR INFORMATION

Corresponding Author

*E-mail: jiangchen@shmu.edu.cn. Tel: +86-21-5198-0079. Fax: +86-21-5198-0079.

Notes

The authors declare no competing financial interest.

■ ACKNOWLEDGMENTS

This work was supported by the grant from National Science Fund for Distinguished Young Scholars (81425023) and National Natural Science Foundation of China (81172993).

■ REFERENCES

(1) Llovet, J. M.; Burroughs, A.; Bruix, J. Hepatocellular Carcinoma. *Lancet* **2003**, *362*, 1907−1917.
(2) Maluccio, M.; Covey, A. Recent Progress in Understanding, Diagnosing, and Treating Hepatocellular Carcinoma. *CA: Cancer J. Clin.* **2012**, *62*, 394−399.
(3) Cervello, M.; McCubrey, J. A.; Cusimano, A.; Lampiasi, N.; Azzolina, A.; Montalto, G. Targeted Therapy for Hepatocellular Carcinoma: Novel Agents on the Horizon. *Oncotarget* **2012**, *3*, 236−260.
(4) Llovet, J. M. Updated Treatment Approach to Hepatocellular Carcinoma. *J. Gastroenterol.* **2005**, *40*, 225−235.
(5) Avila, M. A.; Berasain, C.; Sangro, B.; Prieto, J. New Therapies for Hepatocellular Carcinoma. *Oncogene* **2006**, *25*, 3866−3884.
(6) Villanueva, A. Rethinking Future Development of Molecular Therapies in Hepatocellular Carcinoma: a Bottom-Up Approach. *J. Hepatol.* **2013**, *59*, 392−395.
(7) Hochster, H. S.; Green, M. D.; Speyer, J.; Fazzini, E.; Blum, R.; Muggia, F. M. 4′Epidoxorubicin (Epirubicin): Activity in Hepatocellular Carcinoma. *J. Clin. Oncol.* **1985**, *3*, 1535−1540.
(8) Lai, C. L.; Wu, P. C.; Chan, G. C.; Lok, A. S.; Lin, H. J. Doxorubicin versus No Antitumor Therapy in Inoperable Hepatocellular Carcinoma. A Prospective Randomized Trial. *Cancer* **1988**, *62*, 479−483.
(9) Llovet, J. M.; Real, M. I.; Montana, X.; Planas, R.; Coll, S.; Aponte, J.; Ayuso, C.; Sala, M.; Muchart, J.; Sola, R.; Rodes, J.; Bruix, J. Arterial Embolisation or Chemoembolisation versus Symptomatic Treatment in Patients with Unresectable Hepatocellular Carcinoma: a Randomised Controlled Trial. *Lancet* **2002**, *359*, 1734−1739.
(10) Takemura, G.; Fujiwara, H. Doxorubicin-Induced Cardiomyopathy from the Cardiotoxic Mechanisms to Management. *Prog. Cardiovasc. Dis.* **2007**, *49*, 330−352.
(11) Chatterjee, K.; Zhang, J.; Honbo, N.; Karliner, J. S. Doxorubicin Cardiomyopathy. *Cardiology* **2010**, *115*, 155−162.
(12) Kataoka, K.; Harada, A.; Nagasaki, Y. Block Copolymer Micelles for Drug Delivery: Design, Characterization and Biological Significance. *Adv. Drug Delivery Rev.* **2001**, *47*, 113−131.
(13) Allen, T. M.; Cullis, P. R. Drug Delivery Systems: Entering the Mainstream. *Science* **2004**, *303*, 1818−1822.
(14) Torchilin, V. P. Targeted Polymeric Micelles for Delivery of Poorly Soluble Drugs. *Cell. Mol. Life Sci.* **2004**, *61*, 2549−2559.
(15) Peer, D.; Karp, J. M.; Hong, S.; Farokhzad, O. C.; Margalit, R.; Langer, R. Nanocarriers as an Emerging Platform for Cancer Therapy. *Nat. Nanotechnol.* **2007**, *2*, 751−760.
(16) Matsumura, Y.; Maeda, H. A New Concept for Macromolecular Therapeutics in Cancer Chemotherapy: Mechanism of Tumoritropic Accumulation of Proteins and the Antitumor Agent Smancs. *Cancer Res.* **1986**, *46*, 6387−6392.
(17) Fang, J.; Nakamura, H.; Maeda, H. The EPR Effect: Unique Features of Tumor Blood Vessels for Drug Delivery, Factors Involved, and Limitations and Augmentation of the Effect. *Adv. Drug Delivery Rev.* **2011**, *63*, 136−151.
(18) Ferrari, M. Cancer Nanotechnology: Opportunities and Challenges. *Nat. Rev. Cancer* **2005**, *5*, 161−171.
(19) Ulbrich, K.; Subr, V. Polymeric Anticancer Drugs with pH-Controlled Activation. *Adv. Drug Delivery Rev.* **2004**, *56*, 1023−1050.
(20) Dai, J.; Lin, S.; Cheng, D.; Zou, S.; Shuai, X. Interlayer-Crosslinked Micelle with Partially Hydrated Core Showing Reduction and pH Dual Sensitivity for Pinpointed Intracellular Drug Release. *Angew. Chem., Int. Ed.* **2011**, *50*, 9404−9408.
(21) Li, Y.; Xiao, K.; Zhu, W.; Deng, W.; Lam, K. S. Stimuli-Responsive Cross-linked Micelles for On-Demand Drug Delivery against Cancers. *Adv. Drug Delivery Rev.* **2014**, *66*, 58−73.
(22) Wu, G.; Fang, Y. Z.; Yang, S.; Lupton, J. R.; Turner, N. D. Glutathione Metabolism and Its Implications for Health. *J. Nutr.* **2004**, *134*, 489−492.
(23) Kuppusamy, P.; Li, H.; Ilangovan, G.; Cardounel, A. J.; Zweier, J. L.; Yamada, K.; Krishna, M. C.; Mitchell, J. B. Noninvasive Imaging of Tumor Redox Status and Its Modification by Tissue Glutathione Levels. *Cancer Res.* **2002**, *62*, 307−312.
(24) Allen, T. M. Ligand-Targeted Therapeutics in Anticancer Therapy. *Nat. Rev. Cancer* **2002**, *2*, 750−763.
(25) Torchilin, V. P.; Lukyanov, A. N.; Gao, Z.; Papahadjopoulos-Sternberg, B. Immunomicelles: Targeted Pharmaceutical Carriers for Poorly Soluble Drugs. *Proc. Natl. Acad. Sci. U. S. A.* **2003**, *100*, 6039−6044.
(26) Airley, R. E.; Mobasheri, A. Hypoxic Regulation of Glucose Transport, Anaerobic Metabolism and Angiogenesis in Cancer: Novel Pathways and Targets for Anticancer Therapeutics. *Chemotherapy* **2007**, *53*, 233−256.
(27) Michel, V.; Yuan, Z.; Ramsubir, S.; Bakovic, M. Choline Transport for Phospholipid Synthesis. *Exp. Biol. Med. (Maywood)* **2006**, *231*, 490−504.
(28) Wood, I. S.; Trayhurn, P. Glucose Transporters (GLUT and SGLT): Expanded Families of Sugar Transport Proteins. *Br. J. Nutr.* **2003**, *89*, 3−9.
(29) Warburg, O. On the Origin of Cancer Cells. *Science* **1956**, *123*, 309−314.

DOI: 10.1021/am5091462
ACS Appl. Mater. Interfaces 2015, 7, 5444−5453

(30) Vander, H. M. Targeting Cancer Metabolism: a Therapeutic Window Opens. *Nat. Rev. Drug Discovery* **2011**, *10*, 671−684.
(31) Szablewski, L. Expression of Glucose Transporters in Cancers. *Biochim. Biophys. Acta* **2013**, *1835*, 164−169.
(32) Amann, T.; Hellerbrand, C. GLUT1 as a Therapeutic Target in Hepatocellular Carcinoma. *Expert Opin. Ther. Targets* **2009**, *13*, 1411−1427.
(33) Amann, T.; Maegdefrau, U.; Hartmann, A.; Agaimy, A.; Marienhagen, J.; Weiss, T. S.; Stoeltzing, O.; Warnecke, C.; Scholmerich, J.; Oefner, P. J.; Kreutz, M.; Bosserhoff, A. K.; Hellerbrand, C. GLUT1 Expression is Increased in Hepatocellular Carcinoma and Promotes Tumorigenesis. *Am. J. Pathol.* **2009**, *174*, 1544−1552.
(34) Rodríguez-Enríquez, S.; Marín-Hernández, A.; Gallardo-Pérez, J. C.; Moreno-Sánchez, R. Kinetics of Transport and Phosphorylation of Glucose in Cancer Cells. *J. Cell. Physiol.* **2009**, *22*, 552−529.
(35) Agus, D. B.; Vera, J. C.; Golde, D. W. Stromal Cell Oxidation: a Mechanism by Which Tumors Obtain Vitamin C. *Cancer Res.* **1999**, *59*, 4555−4558.
(36) Rumsey, S. C.; Kwon, O.; Xu, G. W.; Burant, C. F.; Simpson, I.; Levine, M. Glucose Transporter Isoforms GLUT1 and GLUT3 Transport Dehydroascorbic Acid. *J. Biol. Chem.* **1997**, *272*, 18982−18989.
(37) Corti, A.; Casini, A. F.; Pompella, A. Cellular Pathways for Transport and Efflux of Ascorbate and Dehydroascorbate. *Arch. Biochem. Biophys.* **2010**, *500*, 107−115.
(38) Daly, W. H.; Poché, D. The Preparation of *N*-Carboxyanhydrides of α-Amino Acids Using Bis(trichloromethyl)carbonate. *Tetrahedron Lett.* **1988**, *29*, 5859−5862.
(39) Marra, A.; Vecchi, A.; Chiappe, C.; Melai, B.; Dondoni, A. Validation of the Copper(I)-Catalyzed Azide-Alkyne Coupling in Ionic Liquids. Synthesis of a Triazole-linked *C*-Disaccharide as a Case Study. *J. Org. Chem.* **2008**, *73*, 2458−2461.
(40) Reddy, L. H.; Meda, N.; Murthy, R. R. Rapid and Sensitive HPLC Method for the Estimation of Doxorubicin in Dog Blood–the Silver Nitrate Artifact. *Acta Pharm.* **2005**, *55*, 81−91.
(41) Tomayko, M. M.; Reynolds, C. P. Determination of Subcutaneous Tumor Size in Athymic (Nude) Mice. *Cancer Chemother. Pharmacol.* **1989**, *24*, 148−154.
(42) Lallana, E.; Fernandez-Trillo, F.; Sousa-Herves, A.; Riguera, R.; Fernandez-Megia, E. Click Chemistry with Polymers, Dendrimers, and Hydrogels for Drug Delivery. *Pharm. Res.* **2012**, *29*, 902−921.
(43) Bach, L. G.; Islam, M. R.; Nga, T. T.; Binh, M. T.; Hong, S. S.; Gal, Y. S.; Lim, K. T. Chemical Modification of Polyhedral Oligomeric Silsesquioxanes by Functional Polymer via Azide-Alkyne Click Reaction. *J. Nanosci. Nanotechnol.* **2013**, *13*, 1970−1973.
(44) Gindy, M. E.; Ji, S.; Hoye, T. R.; Panagiotopoulos, A. Z.; Prud'Homme, R. K. Preparation of Poly(ethylene glycol) Protected Nanoparticles with Variable Bioconjugate Ligand Density. *Biomacromolecules* **2008**, *9*, 2705−2711.
(45) Parton, R. G.; Simons, K. The Multiple Faces of Caveolae. *Nat. Rev. Mol. Cell Biol.* **2007**, *8*, 185−194.
(46) Okamoto, C. T. Endocytosis and Transcytosis. *Adv. Drug Delivery Rev.* **1998**, *29*, 215−228.
(47) Bottsford-Miller, J. N.; Coleman, R. L.; Sood, A. K. Resistance and Escape from Antiangiogenesis Therapy: Clinical Implications and Future Strategies. *J. Clin. Oncol.* **2012**, *30*, 4026−4034.
(48) Shimanishi, M.; Ogi, K.; Sogabe, Y.; Kaneko, T.; Dehari, H.; Miyazaki, A.; Hiratsuka, H. Silencing of GLUT-1 Inhibits Sensitization of Oral Cancer Cells to Cisplatin during Hypoxia. *J. Oral Pathol. Med.* **2013**, *42*, 382−388.
(49) Robert, J.; Gianni, L. Pharmacokinetics and Metabolism of Anthracyclines. *Cancer Surv.* **1993**, *17*, 219−252.
(50) Lalatsa, A.; Schatzlein, A. G.; Mazza, M.; Le, T. B.; Uchegbu, I. F. Amphiphilic Poly(L-amino acids) - New Materials for Drug Delivery. *J. Controlled Release* **2012**, *161*, 523−536.
(51) Gewirtz, D. A. A Critical Evaluation of the Mechanisms of Action Proposed for the Antitumor Effects of the Anthracycline Antibiotics Adriamycin and Daunorubicin. *Biochem. Pharmacol.* **1999**, *57*, 727−741.

DOI: 10.1021/am5091462
ACS Appl. Mater. Interfaces 2015, 7, 5444−5453